Shadowing Effects on Open and Hidden Heavy Flavor Production at the LHC

R. Vogt

Lawrence Livermore National Laboratory, Livermore, CA 94551, USA
Physics Department, University of California, Davis, CA 95616, USA

Cold Nuclear Matter Effects in Hadroproduction

In heavy-ion collisions, one has to fold in cold matter effects, typically studied in pA or dA interactions from fixed-target energies to colliders

Important cold nuclear matter effects in hadroproduction include:

- **Initial-state nuclear effects on the parton densities (nPDFs)**
- **Initial- (or final-) state energy loss**
- **k_T broadening from multiple scattering**
- **Final-state absorption on nucleons**
- **Final-state break up by comovers (hadrons or partons)**
- **Intrinsic $Q\overline{Q}$ pairs**

After some very brief discussion of each, I will concentrate on nuclear parton densities (shadowing)
Open heavy flavor not affected by absorption or comover interactions

Cold Matter Effects Quantified by A Dependence

Open charm appears to be independent of A ($N_{\rm bin}$) but quarkonium has a definite A dependence

The A dependence includes some or all of the aforementioned nuclear effects

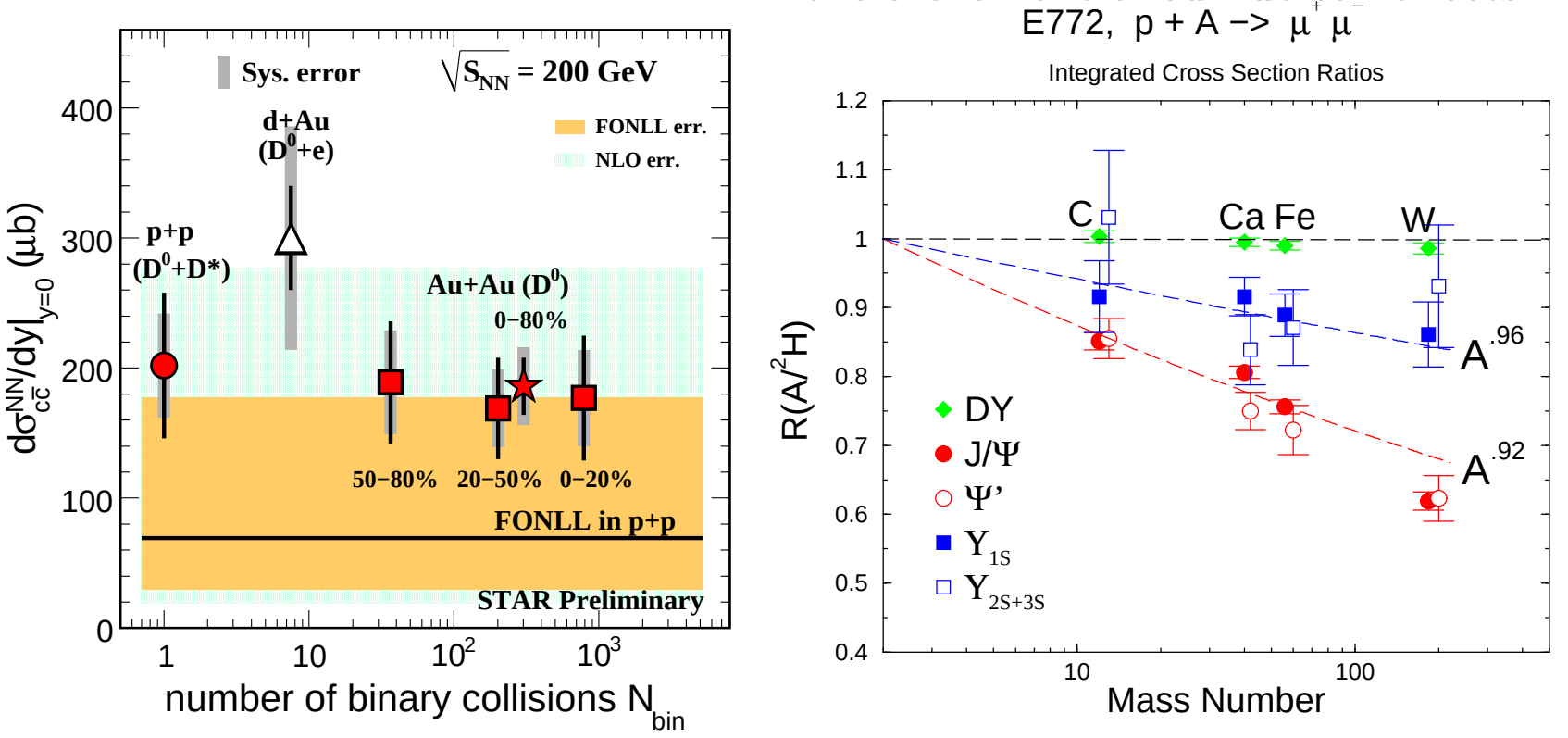

Figure 1: **(Left) The dependence of the open charm cross section on the number of binary collisions measured by the STAR Collaboration at central rapidity. (Right) The A dependence of quarkonium and Drell-Yan production measured by E772.**

E866 Measured Open Charm and J/ψ vs x_F

E866 also measured open charm pA dependence using single muons with $p_T^\mu > 1$ GeV/c (unpublished)

Different from J/ψ for $y < 0.7$ but similar for higher y, suggests that dominant effects are in the initial state

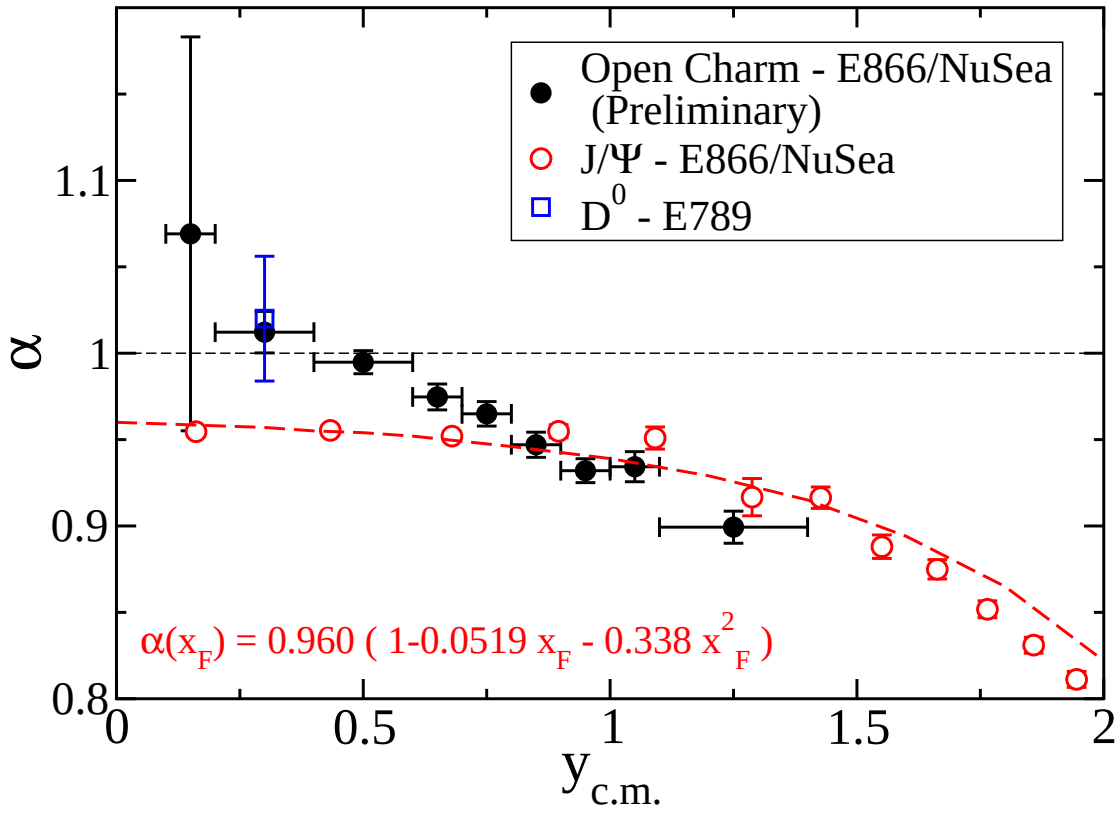

Figure 2: The J/ψ and open charm A dependence as a function of x_F (Mike Leitch).

Quick Tour of Cold Matter Effects

Parton Densities Modified in Nuclei

Nuclear deep-inelastic scattering measures quark modifications directly

More uncertainty in nuclear gluon distribution, only indirectly constrained by Q^2 evolution of parton densities

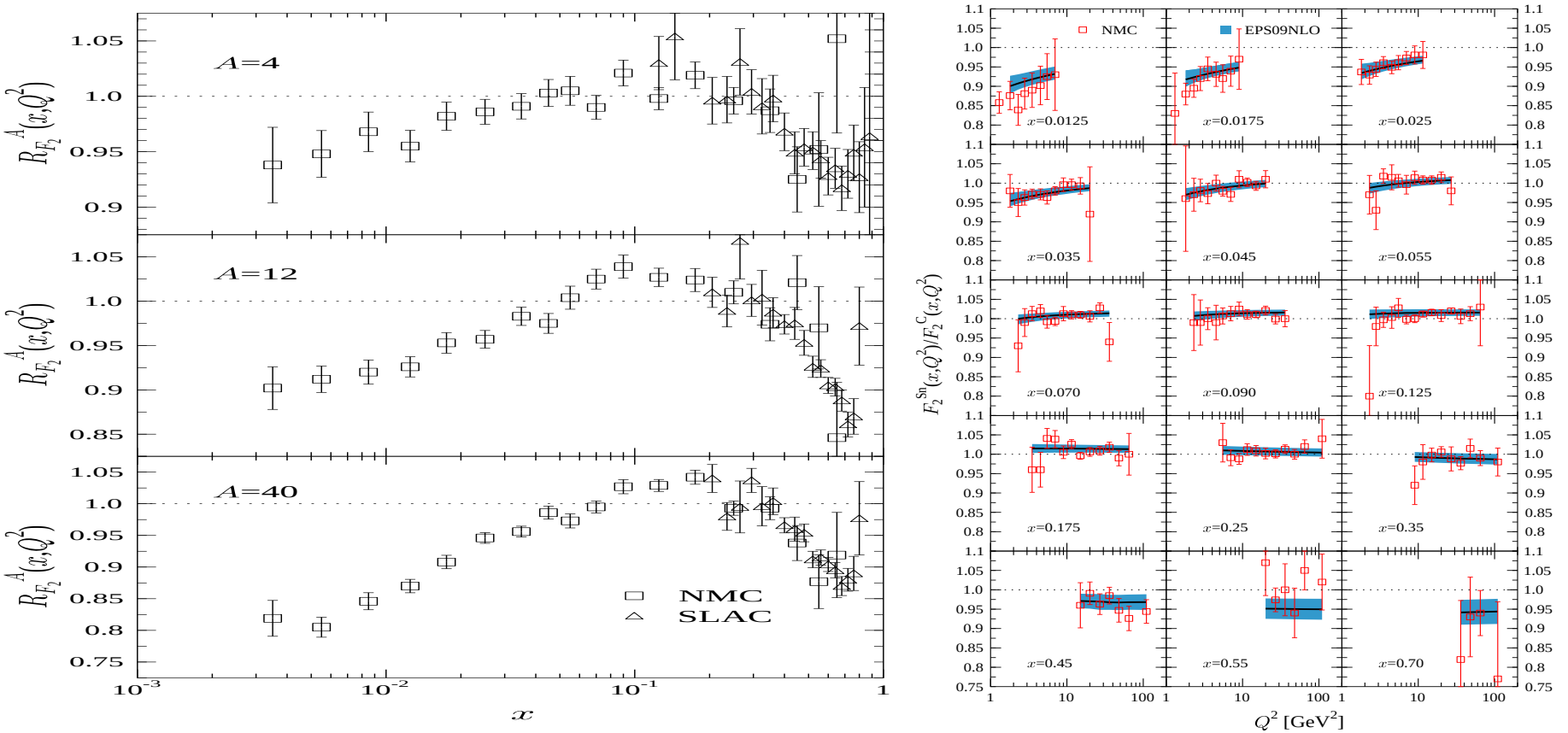

Figure 3: (Left) Ratios of charged parton densities in He, C, and Ca to D as a function of x. (Right) Evolution of gluon distributions in Sn relative to C targets with Q^2 for several fixed values of x. [From K.J. Eskola.]

Why Shadowing Is Not All There Is

Effective α dissimilar as a function of x_2, closer to scaling for $y_{\rm cm}$

At negative x_F, the HERA-B result suggests a negligible effective J/ψ absorption cross section

Argument for more physics at forward x_F than accounted for by nuclear shadowing

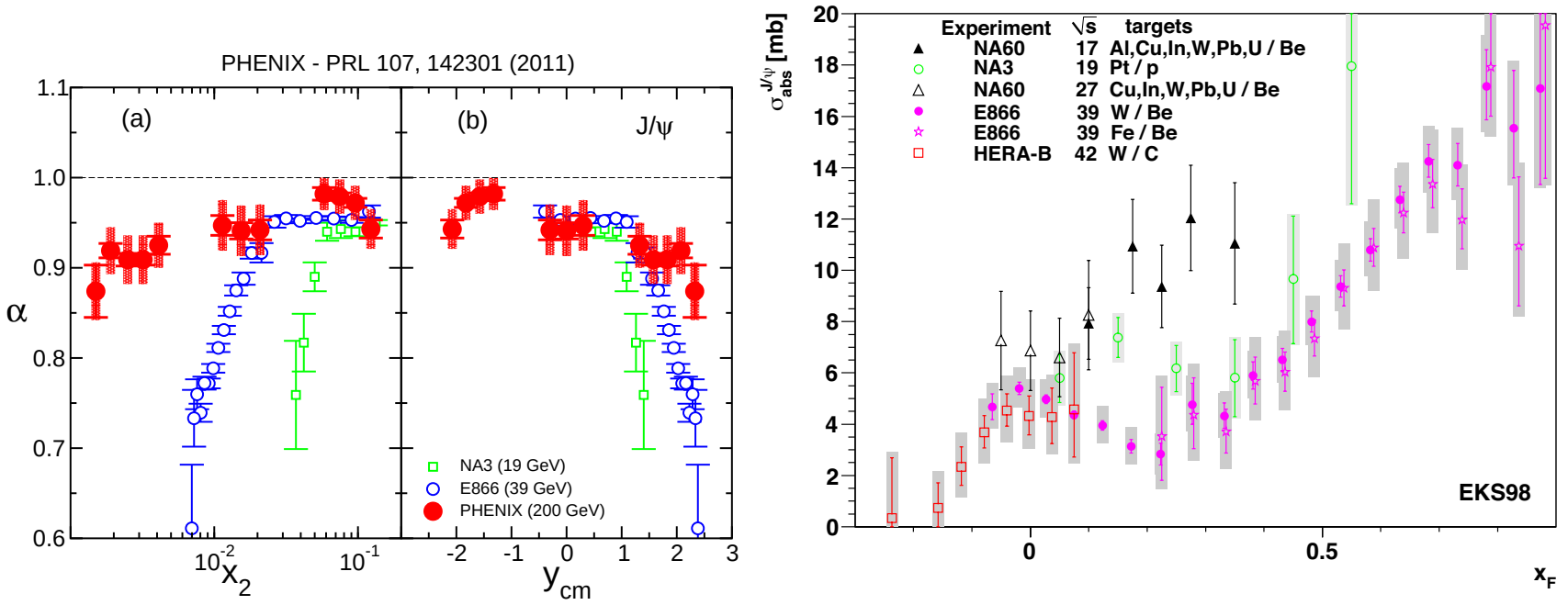

Figure 4: (Left) Comparison of effective α for NA3, E866 and PHENIX. (Mike Leitch) (Right) Comparison of effective $\sigma_{\rm abs}$ for J/ψ (from QWG report, 2010).

Parton Energy Loss Can Describe Trends

Energy loss by multiple scattering in the initial (gluon) or final ($c\overline{c}$) state results in a backward shift in the longitudinal dependence

Same mechanism is responsible for k_T broadening – what's lost to longitudinal kicks increases the average p_T of the final state

Arleo *et al.* used a power law model of pp collisions to implement final-state energy loss on J/ψ, results shown below agree for fixed target interactions, when shadowing is stronger there is a separation

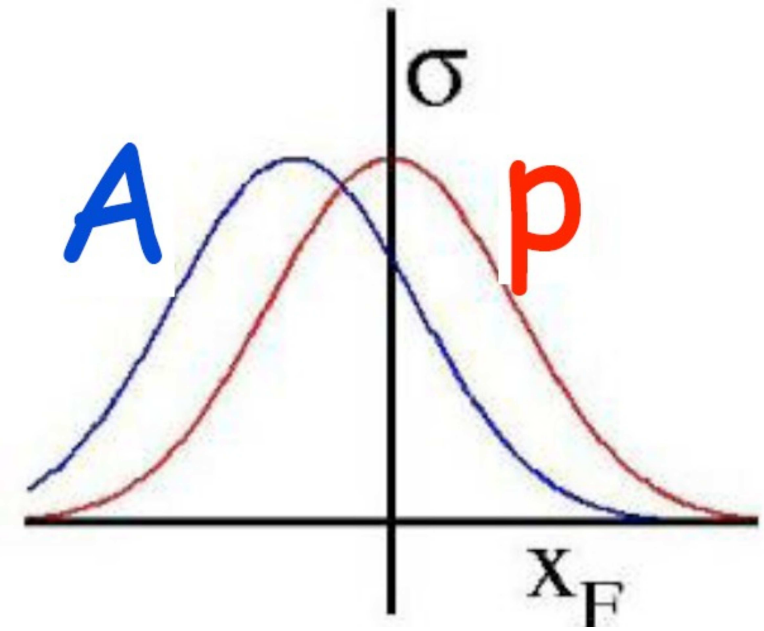

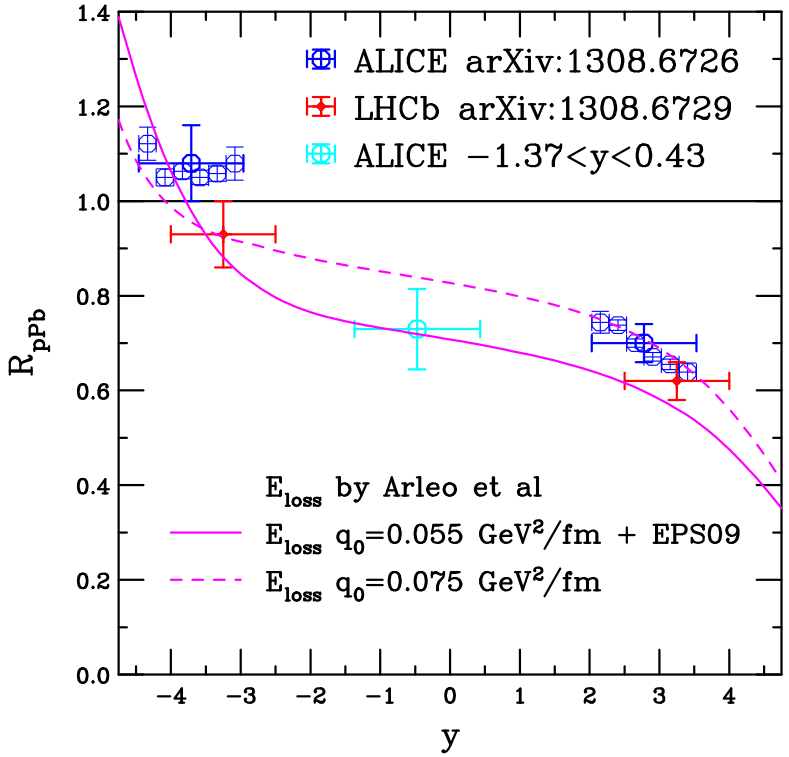

Figure 5: (Left) Shift in x_F distribution caused by energy loss. (Mike Leitch) (Right) The LHC J/ψ $R_{p\mathrm{Pb}}(y)$ data from ALICE and LHCb compared to energy loss model of Arleo *et al.*.

Quarkonium Absorption

Woods-Saxon nuclear density profiles typically used

$$\begin{aligned}\sigma_{pA} &= \sigma_{pN}\int d^2b\int_{-\infty}^{\infty} dz\,\rho_A(b,z)S_A^{\rm abs}(b)\\ &= \sigma_{pN}\int d^2b\int_{-\infty}^{\infty} dz\,\rho_A(b,z)\exp\left\{-\int_z^{\infty} dz'\rho_A(b,z')\sigma_{\rm abs}(z'-z)\right\}\end{aligned}$$

Note that if $\rho_A=\rho_0$, $\alpha = 1-9\sigma_{\rm abs}/(16\pi r_0^2)$

The value of $\sigma_{\rm abs}$ **depends on the whether geometry is taken into account and how realistic that geometry is – hard sphere,** A^α **etc.**

Effective $\sigma_{\rm abs}$ **also depends on whether or not shadowing is taken into account**

Feed down to J/ψ **from** χ_c **and** ψ' **decays included**

$$\sigma_{pA} = \sigma_{pN}\int d^2b\,[0.6S^{\rm abs}_{A\,\psi,\,\rm dir}(b)+0.3S^{\rm abs}_{A\,\chi_{cJ}}(b)+0.1S^{\rm abs}_{A\,\psi'}(b)]$$

Generally assume that each charmonium state interacts with a different, constant asymptotic absorption cross section but, with color singlets, the state grows until it reaches its asymptotic size, NRQCD approach would have different absorption cross sections with different dependence on rapidity, $\sqrt{s}$ **for all states**

The χ_c A **dependence remains unknown (PHENIX measured** $R_{\rm dAu}$ **similar to** J/ψ **but with large uncertainties, no** y **dependence**

A Dependence of J/ψ and ψ' Not Identical

Fixed-target data sets (NA50 at SPS, E866 at FNAL) show clear difference at low x_F (midrapidity)

At RHIC, J/ψ production almost independent of centrality in d+Au collisions while ψ' shows a very strong dependence. Comovers?

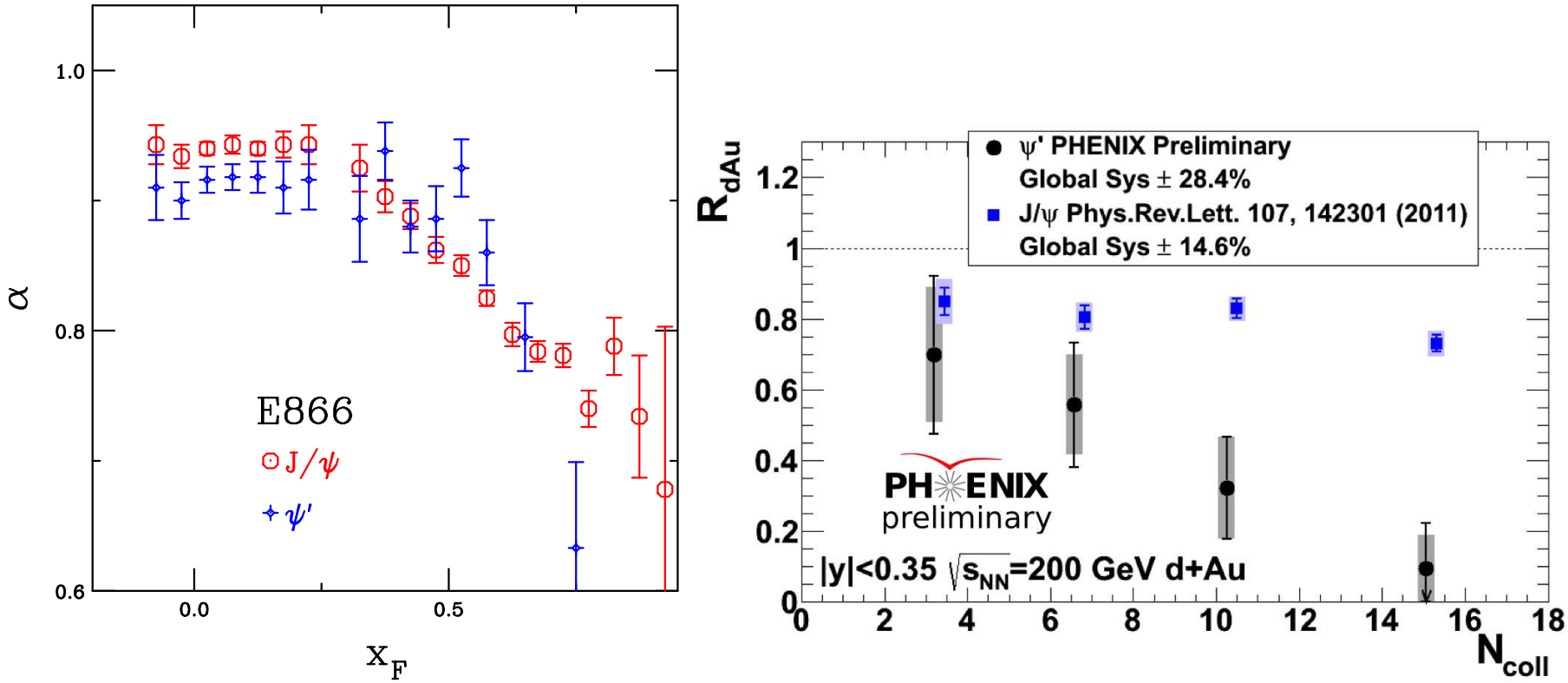

Figure 6: (Left) The A dependence for J/ψ and ψ' production as a function of x_F from E866 at FNAL ($\sqrt{s} = 38.8$ GeV). (Right) The J/ψ and ψ' nuclear modification as a function of collision centrality in d+Au collisions at $\sqrt{s} = 200$ GeV at RHIC.

Effective Absorption Cross Section Energy Dependent

Data corrected for shadowing effects here, dependence of effective absorption cross section on center of mass energy is clear, similar but weaker trend is seen even without shadowing

At the LHC, the absorption cross section is negligible (also, formation time stretched so that charmonium states fully formed outside the nucleus), comovers would be only possible effect

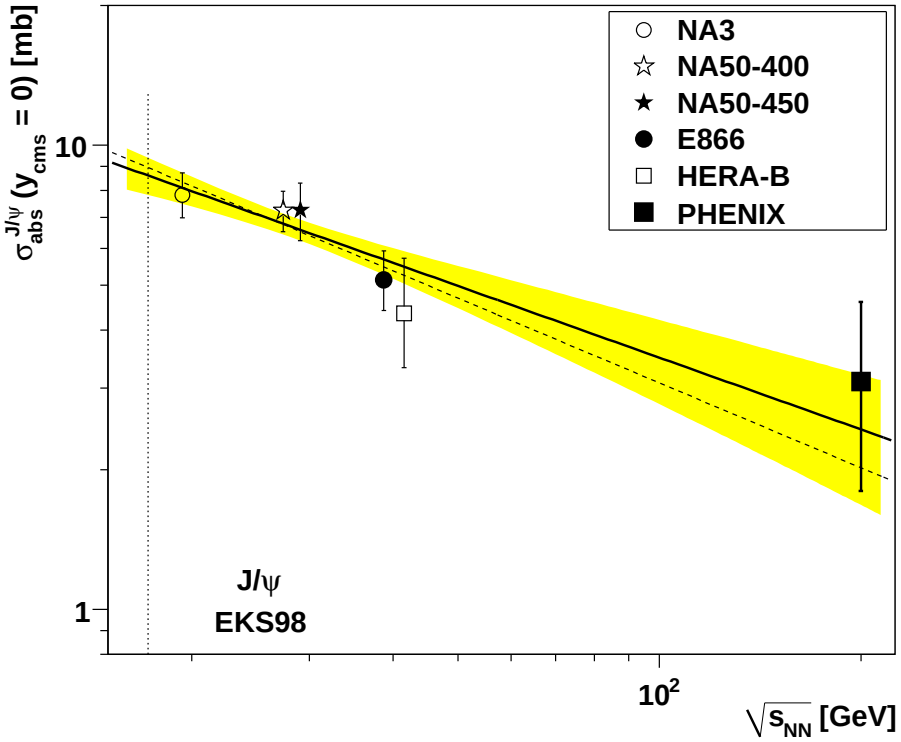

Figure 7: At midrapidity, the effective absorption cross section decreases as a function of energy. (Modified from Lourenco, Wohri and RV.)

Intrinsic Charm

Intrinsic charm long predicted (since 1980's) but difficult to confirm

Several groups have included an intrinsic component in global PDF analyses, Pumplin result from 2007 shown here, latest results from this group similar

IC allowed within each scenario characterized by $\langle x \rangle_{c+\overline{c}}$ at $\mu_0 = 1.3$ GeV,

$$\langle x \rangle_{c+\overline{c}} = \int_0^1 dx\, x\, [c(x) + \overline{c}(x)]$$

Observable consequences on the rapidity distribution at large y, different A dependence (surface relative to volume) causes drop at large x_F (x_1)

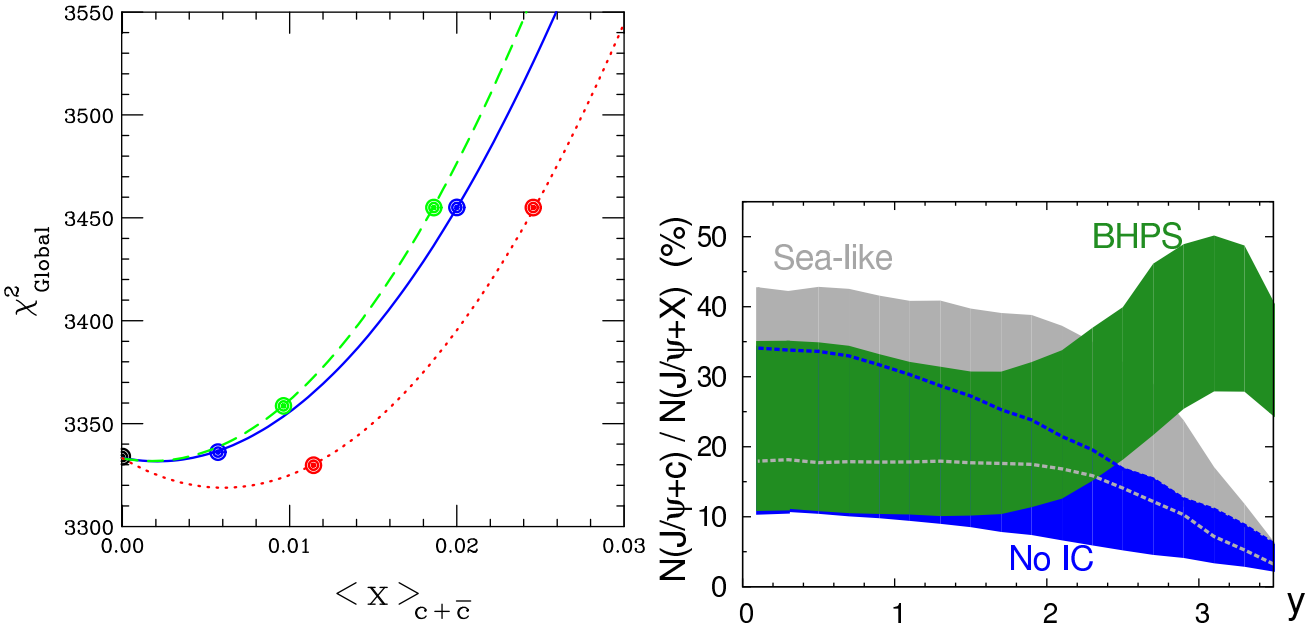

Figure 8: (Left) Goodness of fit for global analyses including IC as a function of $\langle x \rangle_{C+\overline{c}}$ for the light-cone formalism of Brodsky *et al.* (solid), the meson-cloud model (dashed); and sea-like (dotted). The lower dots correspond to candidate fits, 0.057% for Brodsky *et al.*, 0.96% for the meson cloud and 1.1% for sea-like IC. The upper dots are the most marginal fits in the different scenarios, 2% for Brodsky *et al.*, 1.9% for the meson cloud and 2.4% for sea-like. [From Pumplin *et al.*] (Right) Fraction of J/ψ produced in association with a single c-quark ($gc \to J/\psi c$) relative to the direct yield (NLO$^+$) as a function of y_ψ and for no IC, sea-like and Brodsky *et al.* (BHPS). [From Brodsky and Lansberg.]

Shadowing Effects at the LHC

Shadowing Parameterizations Fixed by Global Fits

Most fits (HKN, nDS, DSSZ, EKS, EPS) use available nDIS and Drell-Yan data, along with momentum sum rule and DGLAP evolution to fit a set of parameters modifying the proton PDFs

Example shown is by Eskola and collaborators

Details of fitting and data employed vary but trends are similar

Most fits now available up to NLO, FGS and EPS09s also include impact parameter dependence but other centrality parameterizations also available

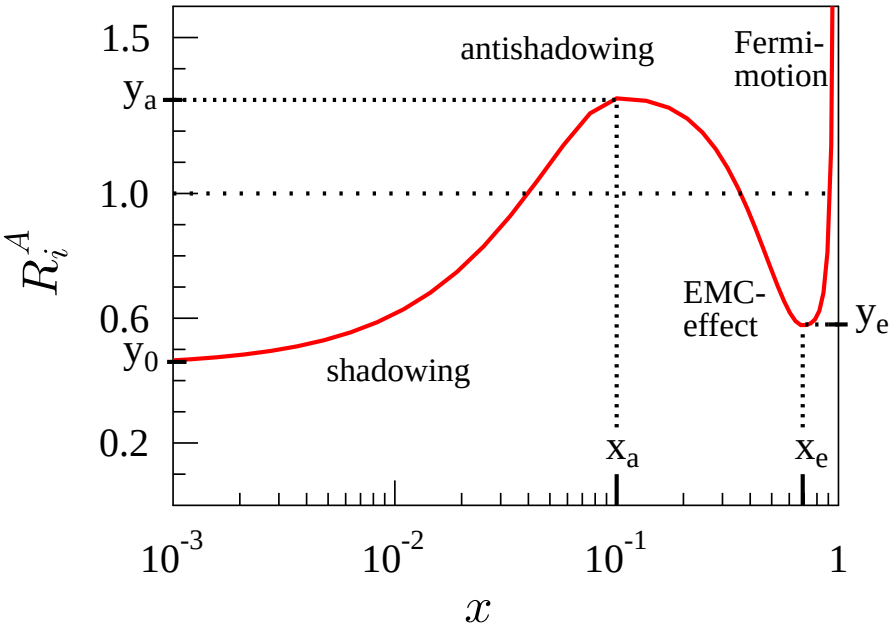

Figure 9: **An illustration of the fit function $R_i^A(x)$ for fits by Eskola *et al.*.**

x Dependence of EPS09

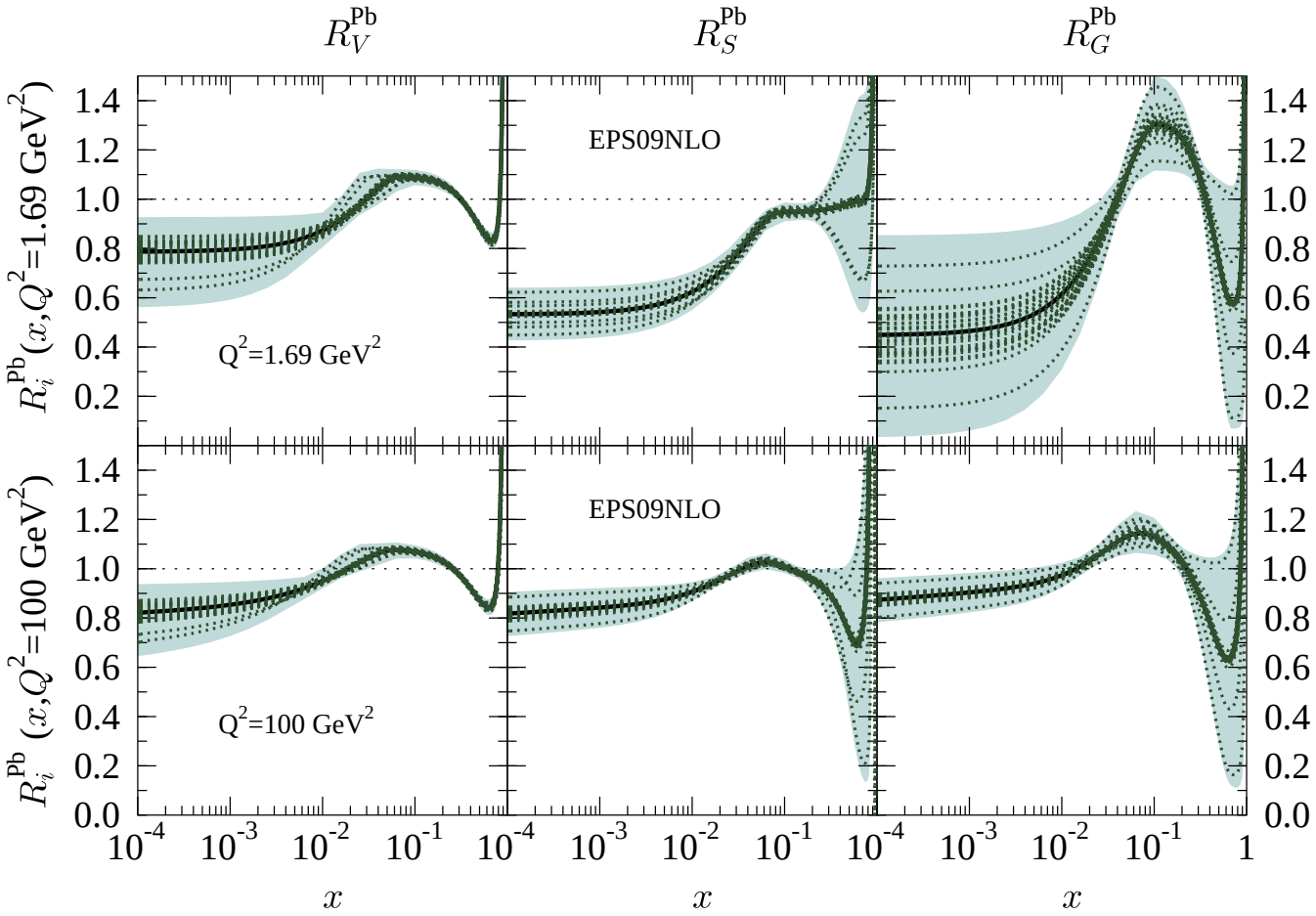

Figure 10: **The x dependence of EPS09 NLO for valence (left), sea (middle) and gluon (right) distributions at $Q^2 = 1.69$ GeV^2 (top), the minimum value of the set, and 100 GeV^2 (bottom) for Pb nuclei. The darkest line in each plot is the central value, the lighter lines are the 30 error sets formed by varying each of the 15 parameters one standard deviation each side of its central value and the shaded region is the full uncertainty band.**

Nuclear PDFs at NLO

x_2 range can reach as low as 10^{-5} in the LHC rapidity acceptance

EPS09 NLO (black) and EKS98 LO (magenta) very similar for $x > 0.002$, significant antishadowing, nDS NLO (blue) and nDSg NLO (red) have almost no antishadowing, nDSg and EKS98 have stronger shadowing than central EPS09 at low x

FGS-H and FGS-L have a minimum x of 10^{-5}, hence the drop

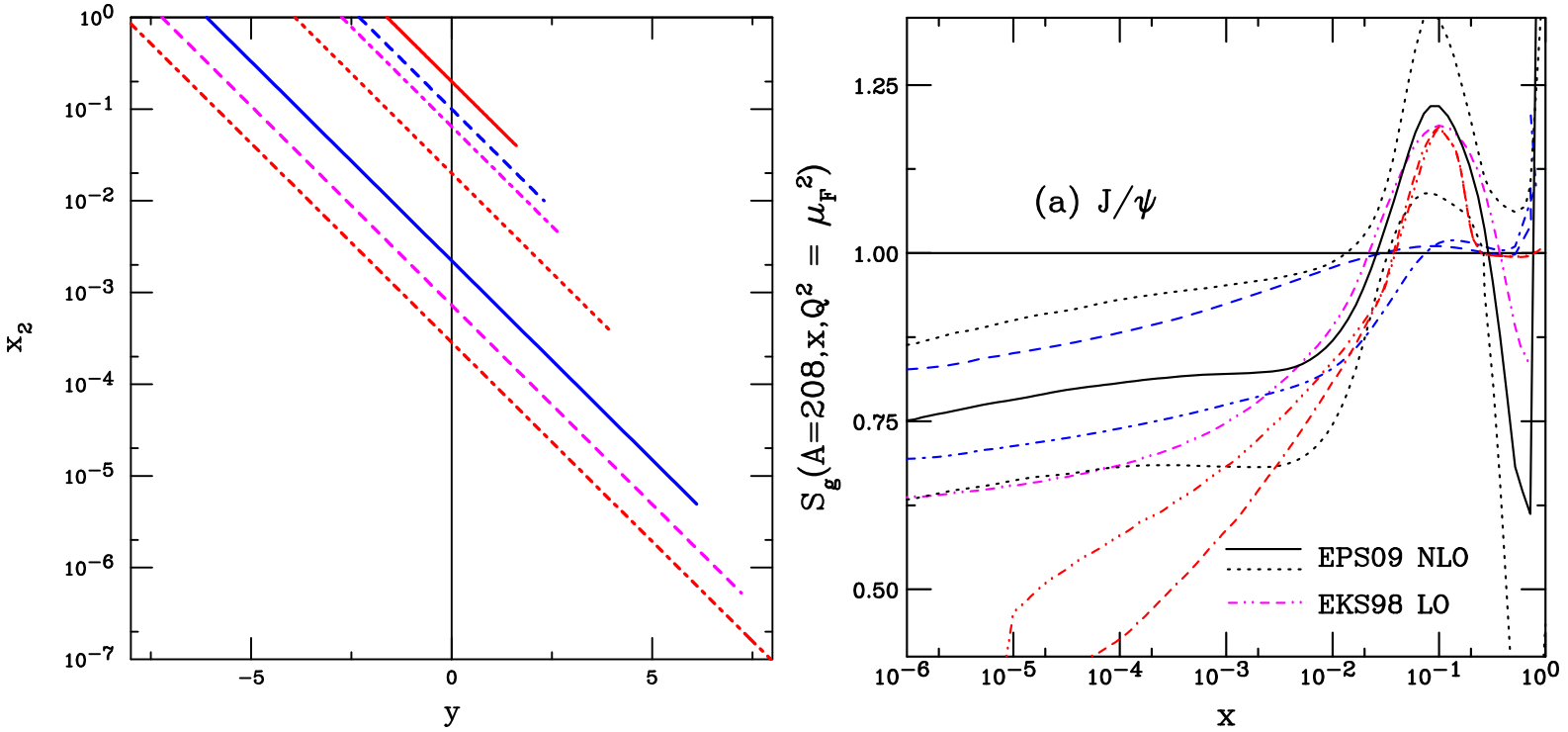

Figure 11: **(Left) The average x_2 as a function of rapidity for $2 \to 2$ scattering (open charm at LO, J/ψ in CEM) for $\sqrt{s} = 20$, 40, 62, 200, 1800, 5500 and 14000 GeV. (Right) Gluon shadowing ratios calculated for Pb nuclei ($A = 208$) calculated at the central value of the fitted factorization scales for J/psi. EPS09 NLO is shown by the black solid curve while the uncertainty band is outlined by the black dotted curves. The NLO nDS and nDSg parameterizations are given in the blue dashed and blue dot dashed curves. The LO EKS98 parameterization is in magenta (dot-dot-dot-dash-dashed). The red dot-dot-dot-dashed and dot-dash-dash-dashed curves are the FGS-L and FGS-H parameterizations respectively.**

Calculating nPDF Uncertainties in pA

EPS09 LO and EPS09 NLO based on CTEQ61L and CTEQ6M respectively

The gluon densities in these two sets differ significantly at low x, hence the low x modifications of EPS09 LO and NLO are quite different

nPDF uncertainties calculated with the 30+1 sets of EPS09: one central set and 30 sets obtained by varying each of the 15 parameters, i.e. sets 2 and 3 were obtained by changing parameter 1 by $\pm 1\sigma_1$ *etc.* where σ_i is the standard deviation of parameter i

Uncertainties due to shadowing calculated using 30+1 error sets of EPS09 NLO added in quadrature so the uncertainty is cumulative

LO and NLO Shadowing Should Agree

LO and NLO shadowing results should agree by construction, as seen for nDS and nDSg

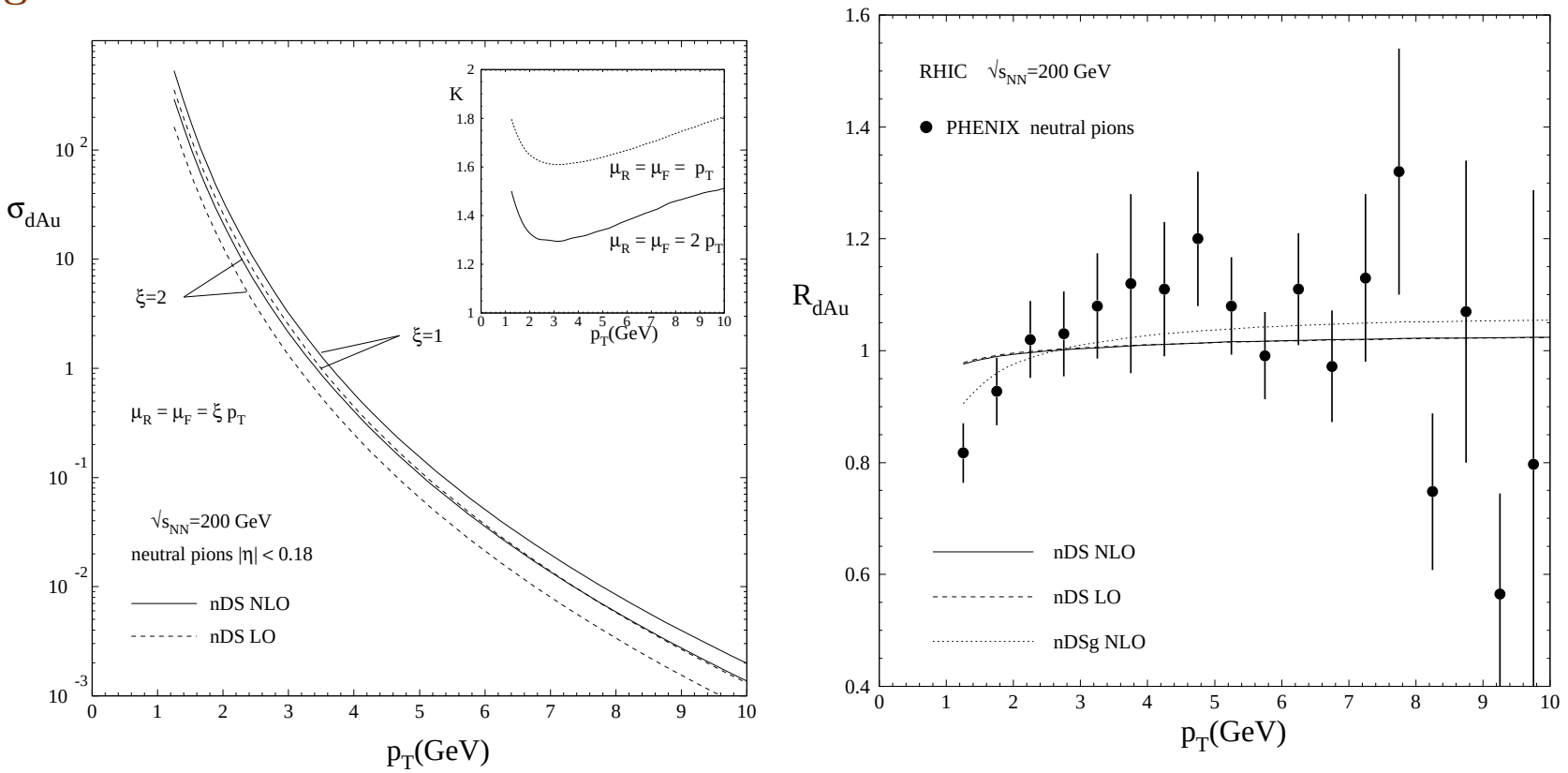

Figure 12: **(Left) The π^0 cross section in d+Au collisions at $\sqrt{s_{NN}} = 200$ GeV at LO and NLO. (Right) The LO and NLO calculations of $R_{\rm dAu}$, along with the NLO calculation with nDSg.**

Results

Open Heavy Flavor

To investigate some nuclear effects, such as k_T broadening, fixed-order scheme required since FONLL only includes fragmentation

Fixed-order MNR code uses Peterson function, $\propto z(1-z)^2/((1-z)^2+\epsilon_Q z)^2$ with $\epsilon_c = 0.06$, $\epsilon_b = 0.006$, much stronger than the FONLL result derived from moments of the fragmentation function.

Fixed-order calculation can include bare quark only; fragmentation only; or broadening with fragmentation – compare to heavy flavor D^0 and D^* meson data from STAR pp collisions at $\sqrt{s} = 200$ GeV

We take various combinations of fragmentation parameters ϵ_Q to match FONLL D meson results and compare/contrast the results of adding an additional k_T kick – the k_T kick was added to the MNR fixed-target calculations because the Peterson fragmentation function was too strong on its own to describe low p_T fixed-target data

Single inclusive charm cross section is finite at $p_T = 0$ so the kick isn't required as it is for quarkonium/heavy flavor pairs – however, it is the only thing that makes the azimuthal distribution between Q and $\overline{Q}$ pair peak away from $\Delta\phi \sim \pi$

Results for LHC at Midrapidity

Test the sensitivity of $R_{p\mathrm{Pb}}$ at midrapidity to the choice of the fragmentation function and amount of k_T broadening

Use standard and reduced values of ϵ_Q, both without and with k_T broadening and calculate $R_{p\mathrm{Pb}}(p_T)$ at midrapidity, including EPS09 NLO parameterization

The $R_{p\mathrm{Pb}}(p_T)$ is only different if we assume higher $\langle k_T^2 \rangle$ in p+Pb than pp

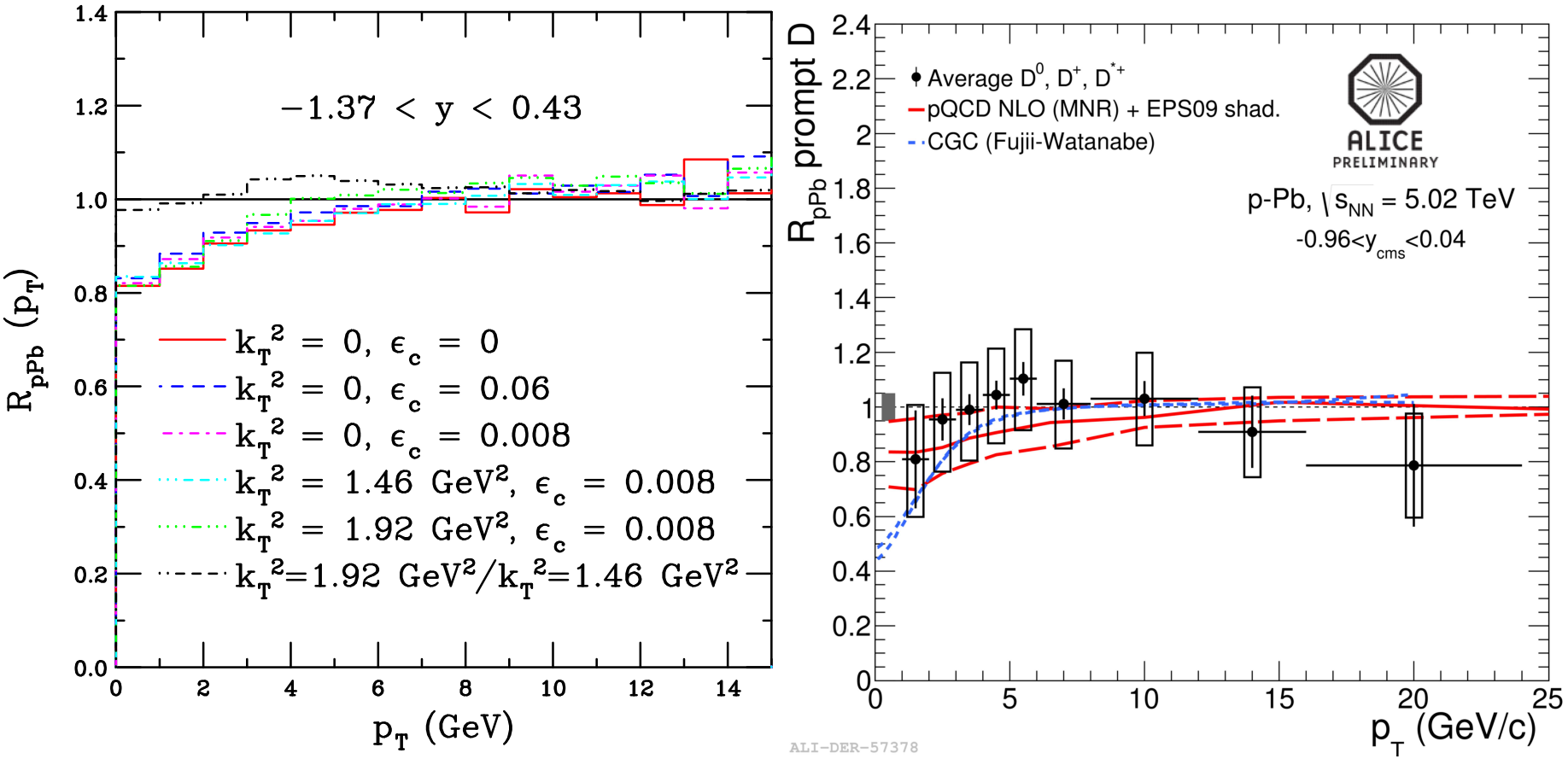

Figure 13: **(Left) The ratio $R_{p\mathrm{Pb}}(p_T)$ for $\sqrt{s_{NN}} = 5$ TeV with EPS09 NLO shadowing only (red), $k_T^2 = 0$ and $\epsilon_c = 0.06$ (blue), $k_T^2 = 0$ and $\epsilon_c = 0.008$ (magenta), $k_T^2 = 1.46$ GeV^2 and $\epsilon_c = 0.008$ (cyan) and $k_T^2 = 1.92$ and $\epsilon_c = 0.008$ (green). The last result (black) assumes a larger intrinsic k_T kick in p+Pb than in pp. (Right) The ratios relative to pp, assuming the same k_T kick and fragmentation value of ϵ_c in p+Pb and pp except for the last calculation where the k_T kick is assumed to be larger in p+Pb. (Right) The ALICE results for D mesons.**

EPS09 Uncertainty Bands I: $R_{p\mathrm{Pb}}(p_T)$

Data typically show stronger effect than central EPS09 result alone but the data tend to fall within the uncertainty band

These calculations (also for the rapidity dependence, next slide) differ somewhat from previous results shown – the wrong scale was being passed to the nPDFs

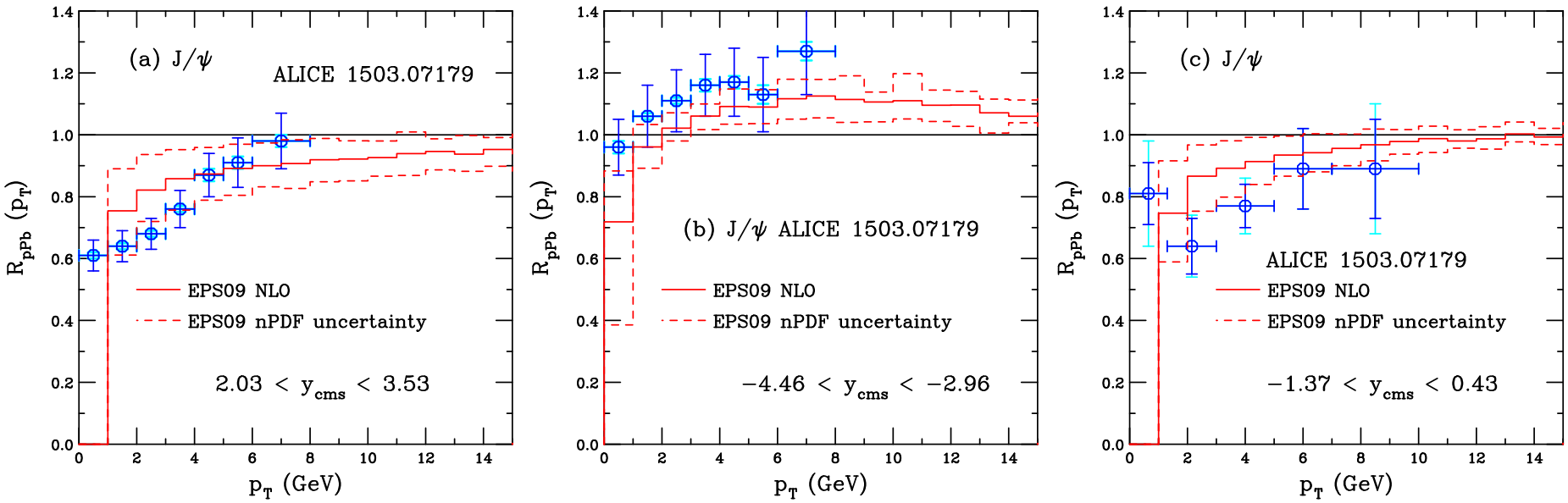

Figure 14: **The ratio $R_{p\mathrm{Pb}}(p_T)$ for ALICE at forward rapidity (left) and backward (middle) and central (right) rapidity. The EPS09 uncertainty band is shown.**

EPS09 Uncertainty Bands II: $R_{p\mathrm{Pb}}(y)$, R_{FB}

Backward rapidity data agree with the rise at $y < -2.5$ from antishadowing onset

Midrapidity and forward rapidity data are consistent with the lower edge of the band only

Reduced uncertainties in the forward/backward ratio because we take the ratio before adding differences in quadrature

The p_T ratio almost flat and above the data for $p_T < 6$ GeV

Curvature of rapidity ratio at $y > 2.5$ reflects the antishadowing rise at backward rapidity and the narrower uncertainty band in this region relative to the forward region

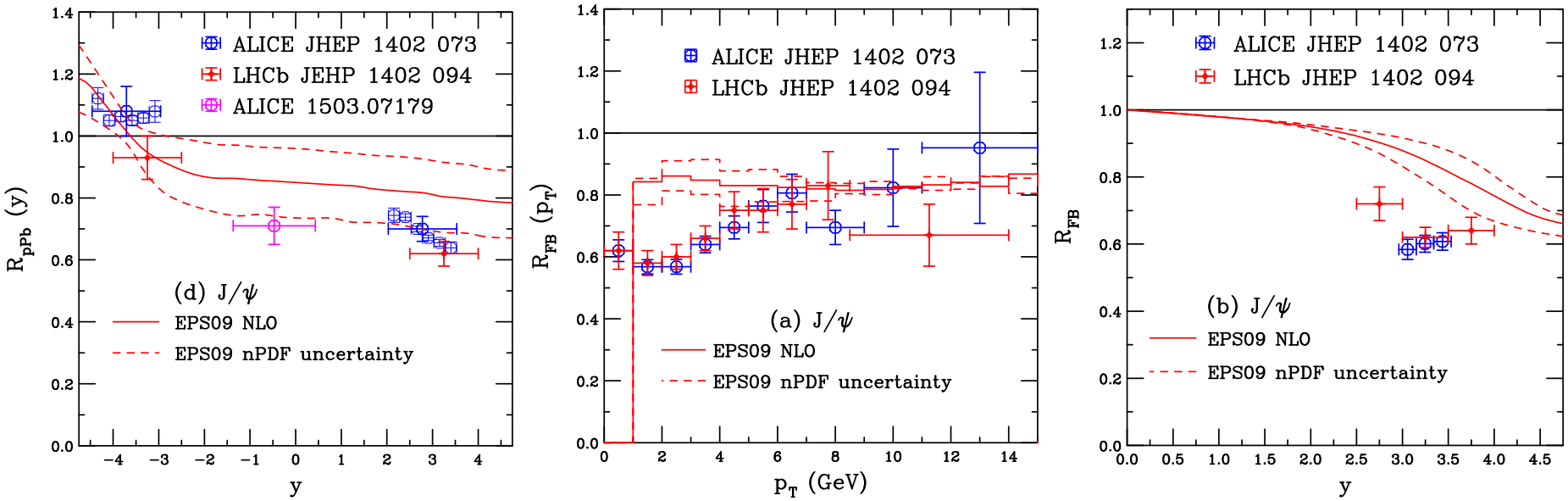

Figure 15: **(Left) The EPS09 NLO uncertainty band, $R_{p\mathrm{Pb}}(y)$. The ratio $R_{FB}(p_T)$ for ALICE (center) and $R_{FB}(y)$ (right). The EPS09 uncertainty band is shown.**

NLO vs LO: EPS09

The nPDF set should be appropriate to the order of the calculation: if using the LO set in a NLO calculation agrees better with the data, it isn't really better

NLO calculation required for CEM p_T distribution and is more appropriate

LO CEM uncertainty band is broader, with stronger shadowing, to counterbalance the flatter low x behavior of CTEQ61L while CTEQ6M is valence-like: different behavior of proton PDFs makes good order-by-order agreement of $R_{p\mathrm{Pb}}$ difficult

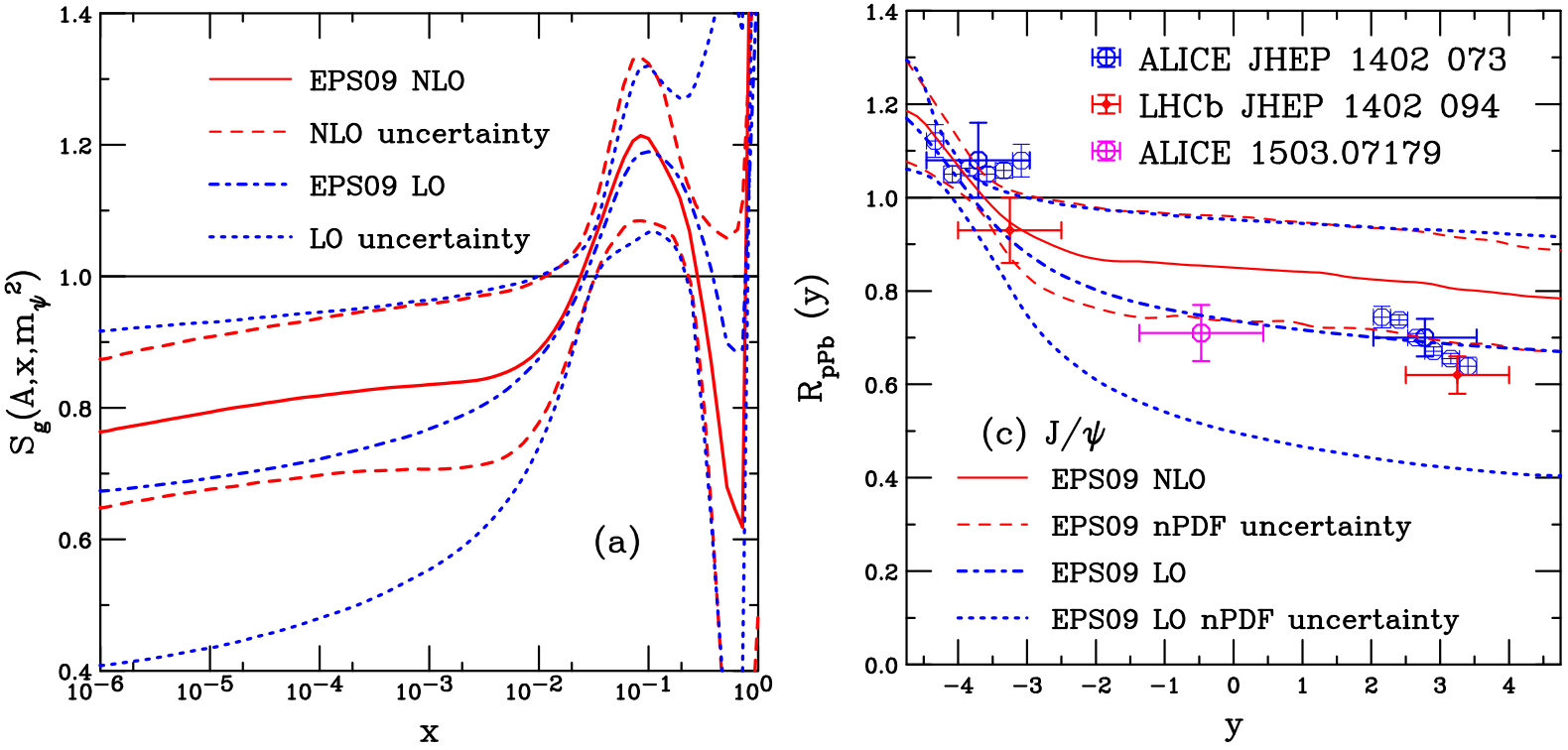

Figure 16: **(Left) The EPS09 LO (blue) and NLO (red) uncertainty bands for gluon shadowing. The corresponding uncertainty bands for $R_{p\mathrm{Pb}}(y)$ at $\sqrt{s_{NN}} = 5$ TeV for J/ψ (right).**

NLO vs LO: nDS

While there are some differences between the LO and NLO nDS and nDSg ratios, especially for nDSg at $x \sim 0.01$, the LO and NLO ratios are much closer than those of the EPS09 central sets, here order of calculation is not an issue

nDS(g) employs GRV98 LO and NLO proton PDFs, the Q^2 range of the nPDF, $1 < Q^2 < 10^6$ GeV^2, is above the minimum scale of GRV98, unlike EPS09 and CTEQ6

Here LO and NLO are consistent

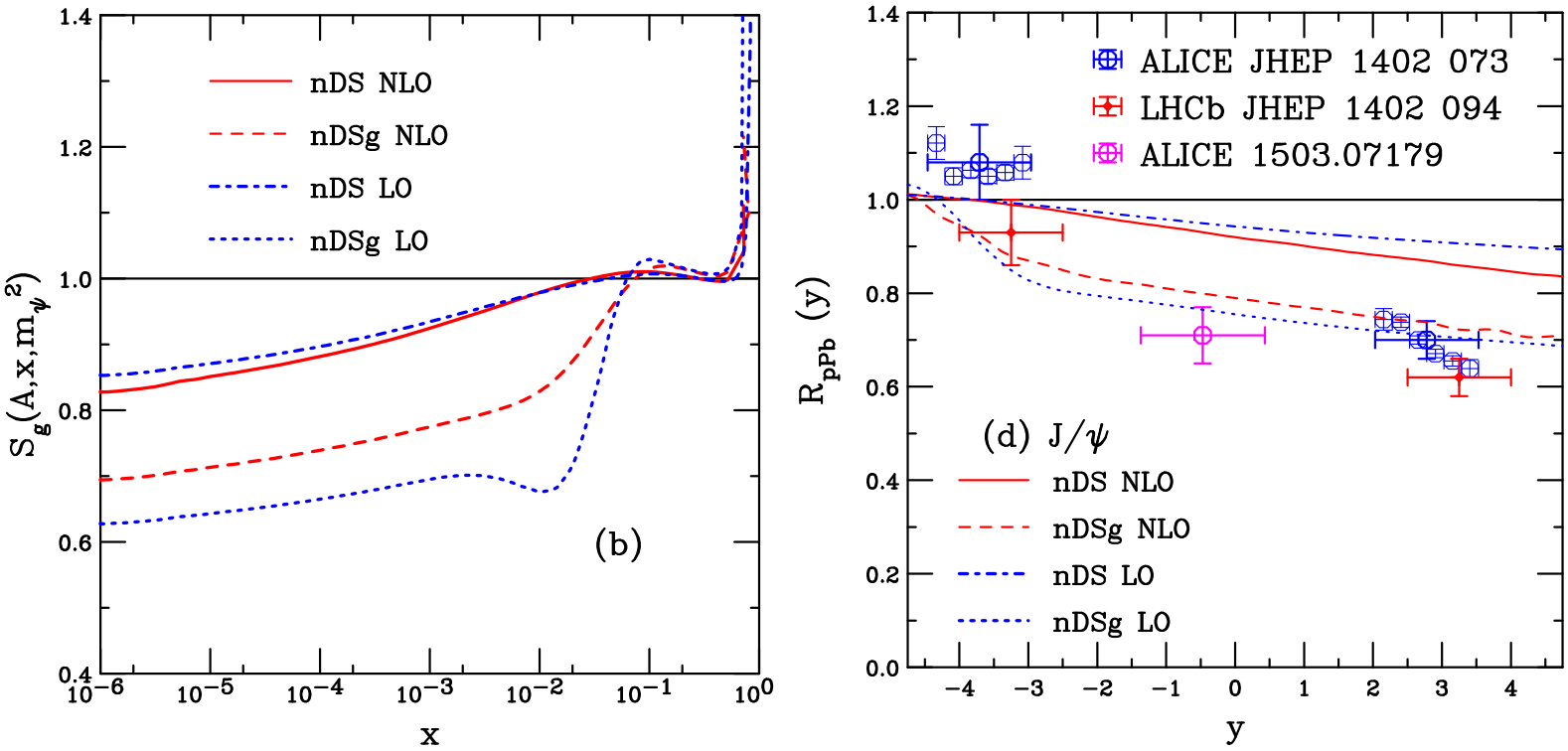

Figure 17: **(Left) The nDS and nDSg LO (blue) and NLO (red) gluon shadowing ratios. The corresponding results for $R_{p\mathrm{Pb}}(y)$ at $\sqrt{s_{NN}} = 5$ TeV are shown for J/ψ (right).**

EPS09 vs Other nPDFs I: $R_{p\mathrm{Pb}}(p_T)$

Central EPS09 NLO set compared to nDS NLO, nDSg NLO and EKS98 (LO)

nDS effect is weakest of all while nDSg is weak at backward rapidity but stronger than EPS09 at mid- and forward rapidity

EKS98 and EPS09 NLO are very similar for $x > 0.01$ so they agree well at backward and mid-rapidity while EKS98 is stronger at forward rapidity

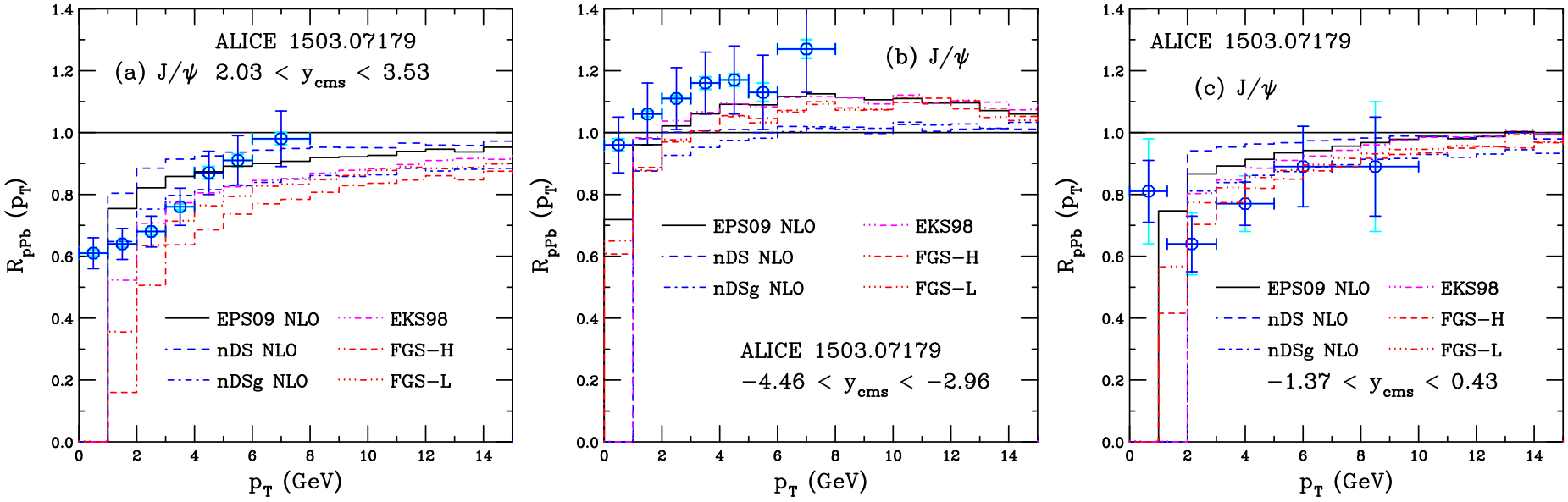

Figure 18: **The ratio $R_{p\mathrm{Pb}}(p_T)$ for ALICE at forward (left), backward (center) and mid- (right) rapidity. The ratios are for central EPS09 NLO (black), nDS NLO (blue dashed), nDSg NLO (blue dot dashed), EKS98 LO (magenta), FGS-H NLO (red dot-dash-dash-dashed) and FGS-L NLO (red dot-dot-dot-dashed).**

EPS09 vs Other nPDFs II: $R_{p\mathrm{Pb}}(y)$, R_{FB}

EKS98 LO follows EPS09 NLO central set until $y > -2$ where it decreases linearly while EPS09 becomes flatter

nDS and nDSg, with no antishadowing, have a weaker y dependence overall

FGS-H and FGS-L show strong drop at $y > 3.7$ occurs where $x_2 \leq 10^{-5}$

nDS has strongest p_T dependence of $R_{FB}(p_T)$, EKS98 comes closest to agreement with low p_T data due to the stronger effect at low x than EPS09

Only EPS09 shows curvature in $R_{FB}(y)$, the others show an almost linear y dependence (aside from far forward 'feature of FGS)

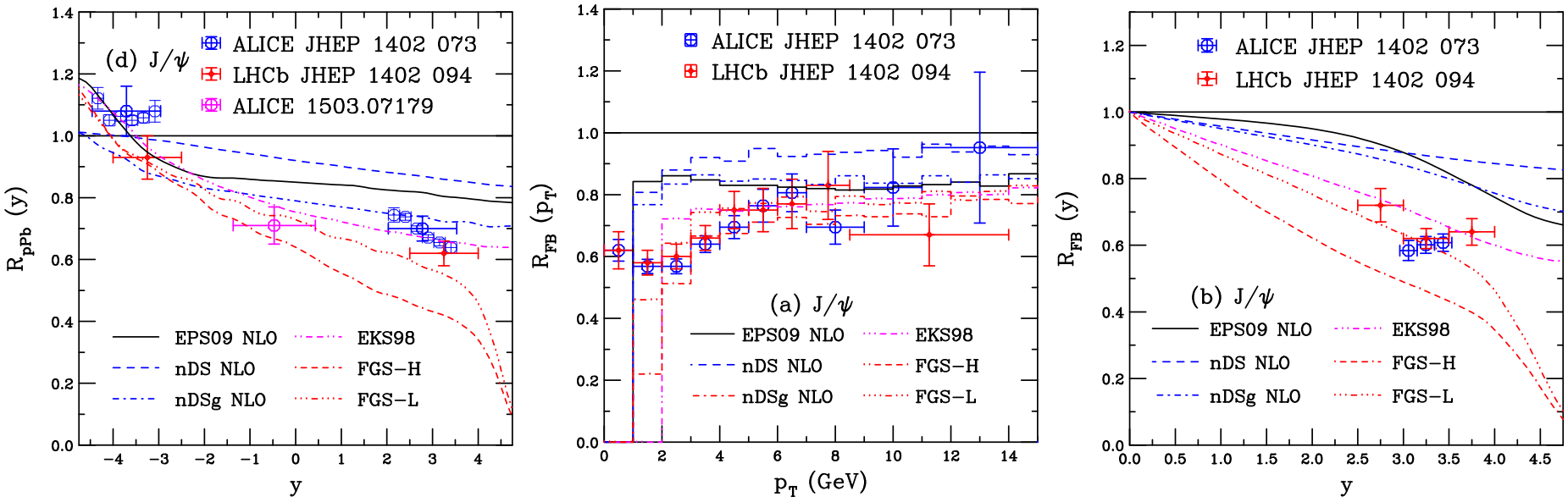

Figure 19: **(Left) The calculated $R_{p\mathrm{Pb}}(y)$ for central EPS09 NLO (black), nDS NLO (blue dashed), nDSg NLO (blue dot dashed), EKS98 LO (magenta), FGS-H NLO (red dot-dash-dash-dashed) and FGS-L NLO (red dot-dot-dot-dashed). The ratio $R_{FB}(p_T)$ for ALICE (center) and $R_{FB}(y)$ (right). The ratios are for central EPS09 NLO (black), nDS NLO (blue dashed), nDSg NLO (blue dot dashed), EKS98 LO (magenta), FGS-H NLO (red dot-dash-dash-dashed) and FGS-L NLO (red dot-dot-dot-dashed).**

Summary

- **Numerous cold matter effects have been postulated, shadowing is important but proportion is unclear**
- **Differences in LO and NLO results for EPS09 on J/ψ production illustrates the fact that gluon nPDF is still not very well constrained, although, given the approximate concordance of the nDS results, the EPS09 discrepancy may be due to the choice of CTEQ6 proton PDFs**
- **LHC p+Pb hadroproduction data could be taken into global analyses in the future but many caveats on medium effects, *e.g.* initial and/or final state energy loss, production mechanism, saturation effects – while the $R_{p\mathrm{Pb}}$ results, both as a function of p_T and y, look good, the R_{FB} results are not as good: pp data at 5 TeV are required**